JOURNAL
OF THE AMERICAN CHEMICAL SOCIETY

VOLUME 101, NUMBER 20 SEPTEMBER 26, 1979

# Stereoelectronic Effects in the Reactions of Phosphate Diesters. Ab Initio Molecular Orbital Calculations of Reaction Surfaces. 2

**David G. Gorenstein,*[1] Bruce A. Luxon, and John B. Findlay**

*Contribution from the Department of Chemistry, University of Illinois at Chicago Circle, Chicago, Illinois 60680.* *Received April 16, 1979*

**Abstract:** Ab initio molecular orbital calculations of the reaction profile for hydroxide-catalyzed hydrolysis of dimethyl phosphate in a number of different conformations reveal large stereoelectronic effects. In the two-step reaction, proceeding via a metastable pentacovalent phosphorane intermediate, both hydroxide attack and methoxide displacement steps are stereoelectronically controlled. Antiperiplanar lone pairs on the basal ester oxygen in the trigonal bipyramidal transition states facilitate translation of the apical bond. In contrast to previous studies on the stereoelectronic effect, orientation of the leaving bond does *not* alter the energy of the transition state.

## Introduction

Stereoelectronic control, or the role of orbital orientation in organic and enzymatic reactions, has been of considerable current interest.[2-10] Deslongchamps and co-workers[2] have demonstrated selective cleavage of bonds which are antiperiplanar (app) to lone pairs on directly bonded oxygen and nitrogen atoms in tetrahedral carbon species. Research groups of Lehn,[5,6] Pople,[7] Gorenstein,[8-10] and others[11] have provided theoretical justification for these stereoelectronic effects in tetracovalent carbon species and phosphates and pentacovalent phosphoranes.

We have recently suggested that this stereoelectronic effect is responsible for a selective weakening of P-O ester bonds which are app to lone pairs on directly bonded oxygen atoms. The theory may provide an important basis for further understanding enzymatic[8] and nonenzymatic[9,10] reactions of phosphate esters. It is suggested that a significant portion of the $10^6$-$10^8$-fold rate acceleration of five-membered cyclic phosphates relative to acyclic phosphates derives from this stereoelectronic effect.[9] In addition, in a preliminary communication we presented an ab initio molecular orbital study on a stereoelectronically controlled reaction surface for the base-catalyzed hydrolysis of dimethyl phosphate. Although several other molecular orbital calculations on the reactions of phosphate esters have been reported,[12-16] the previous communication[10] and the present paper represent the first ab initio investigation of stereoelectronic effects in the oxyphosphorane mechanism of phosphate ester hydrolysis. While most of the previous ideas about stereoelectronic effects have been supported, additional calculations are provided in the present work which contradict Lehn and Wipff's[5,6] and our own conclusions[9,10] that orientation about the leaving group leads to significant stereoelectronic effects.

## Methods of Calculation

The SCF LCAO-MO ab initio calculations utilized the GAUSSIAN 70 series of programs with a STO-3G minimal basis set[17a] (no 3d polarization functions on phosphorus). The electron density difference plot was calculated using the program MOPLOT.[17b]

Initial structures for dimethyl phosphate monoanion (DMP) and dimethoxyphosphorane (DMPane) were modeled on the basis of X-ray crystallographic structures of appropriate molecules. The molecular geometry of DMP was optimized by sequentially varying a set of geometrical parameters until the total energy had been effectively minimized. Key parameters were selected from the initial idealized geometry and optimized iteratively until it was clear that only very small (<0.02 kcal/mol) decreases in energy were possible by further calculation.

It is well known that the values of optimized scale factors (and therefore charge distributions) can vary a great deal for a given atom in different molecules,[18] so before optimizing the geometry it was decided to optimize the scale factors of the atoms in the phosphate tetrahedron. Only the valence shell scale factors were optimized and then sequentially in three groups—phosphorus 3sp, ester oxygen 2sp, and phosphoryl oxygen 2sp (values are shown in Table I). It was at this point that the optimization of geometry was initiated. The sequence of geometry optimization was (1) O-P-O bond angle, $\theta$; (2) ester P-OR bond lengths, $r_1$; (3) phosphoryl O-P-O bond angle, $\phi$; (4) phosphoryl P-O bond lengths, $r_3$; (5) $\theta$ again; (6) C-O-P bond angle, $\psi$; finally (7) the RO-POR torsional angles $\omega$, $\omega'$. The final geometries are given in Table II (see Figure 1 for a definition of the geometrical parameters).

Using the reoptimized scale factors shown in Table I, geometry optimization for the stable dimethoxyphosphorane intermediates, **2**, proceeded similarly, with the geometric parameters (see Figure 2) sequentially varied until the final geometries shown in Table III were obtained. The phosphorane oxygens were constrained to $C_s$ symmetry during this minimization.

An initial search for the transition state for the attack of hydroxide on the DMP suggested that the partially optimized geometry with $d_{P\text{-}OH}$ = 2.5 Å was a realistic choice for the

0002-7863/79/1501-5869$01.00/0  

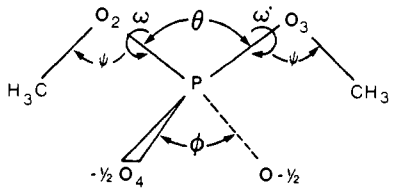

1

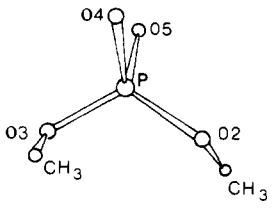

1a (g,g)

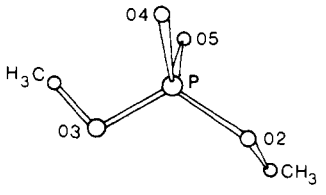

1b (g,t)

Figure 1. Definition of geometrical parameters for dimethyl phosphate monoanion, 1. Top structure shown is in the trans, eclipsed conformation, $\omega = \omega' = 180°$.

Table I. Optimized[a] P and O Valence Shell Scale Factors

| atom (orbital) | DMP | DMPane intermediate 2 | DMPane $^-OH$ attack 3 | DMPane $^-OCH_3$ leaving 4 |
|---|---|---|---|---|
| P (3sp) | 2.033 | 2.023 | 2.023 | 2.023 |
| $O_2$ (2sp) | 2.206 | 2.194 | 2.194 | 2.111 |
| $O_3$ (2sp) | 2.206 | 2.204 | 2.204 | 2.204 |
| $O_{4,5}$ (2sp) | 2.127 | 2.098 | 2.098 | 2.098 |
| $O_6$ (2sp) | 2.104[b] | 2.182 | 2.111 | 2.182 |

[a] Initial values $\zeta_{3sp}(P) = 1.90$, $\zeta_{2sp}(O) = 2.25$. [b] As $^-OH$ at ≥20 Å from DMP.

Table II. Geometries for the Staggered Torsional Conformations of Dimethyl Phosphate Monoanion

| parameter[a] | 1a (g,g) | 1b (g,t) |
|---|---|---|
| Bond Lengths (Å) | | |
| P-$O_2$ ($r_1$) | 1.667 | 1.666[b] |
| P-$O_3$ ($r_1$) | 1.667 | 1.667[c] |
| P-$O_{4,5}$ ($r_3$) | 1.538 | 1.538 |
| C-O ($r_2$) | 1.43 | 1.43 |
| C-H[d] | 1.09 | 1.09 |
| Bond Angles (deg) | | |
| $O_2$-P-$O_3$ ($\theta$) | 98.81 | 94.90 |
| $O_4$-P-$O_5$ ($\phi$) | 125.66 | 124.30 |
| P-O-C ($\psi$) | 112.41 | 111.75 |
| O-C-H[d] ($\alpha$) | 109.5 | 109.5 |
| H-C-H[d] ($\beta$) | 109.5 | 109.5 |
| Dihedral Angles (deg) | | |
| C-$O_2$-P-$O_3$ ($\omega$) | 68.2 | 74.6 |
| C-$O_3$-P-$O_2$ ($\omega'$) | 68.2 | 179.2 |
| P-$O_{2,3}$-C-H[d] | 180.0 | 180.0 |

[a] See Figure 1 for definition of geometrical parameters. $C_{2v}$ symmetry assumed for P-O framework. [b] Gauche bond. [c] Trans bond. [d] Assumed.

transition state. Extensive geometry optimization as for the dimethoxyphosphorane on this structure with $d_{P\text{-}OH} = 2.5$ Å was performed and the results are shown in Table IV. The geometries for the methoxide displacement transition states

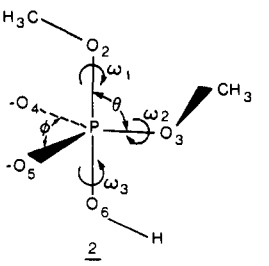

2

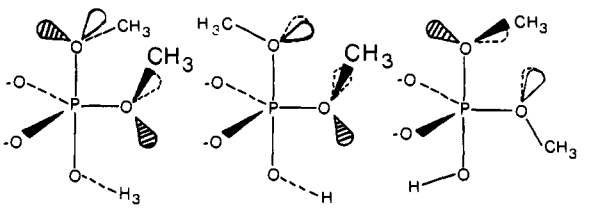

2a (g,g,-g) 2b (t,g,-g) 2c (g,t,t)

Figure 2. Definition of geometrical parameters for dimethoxyphosphorane intermediates, 2. Torsional angles about the P-OMe bonds for 2 are defined by the MeOPOMe structural fragment and the torsional angle about the P-OH bond is defined by the MeO(3)POH fragment. Conformers are defined by the following order for the torsional angles: apical O(2) ester, equatorial O(3) ester, and apical P-O(6)H bonds. Conformations (g,g, −g), (t,g, −g), and (g,t,t) are shown with antiperiplanar lone pairs shaded.

Table III. Geometries for the Various Dimethoxyphosphorane Intermediates

| parameter[a] | 2a (g,g, −g) | 2b (t,g, −g) | 2c (g,t,t) |
|---|---|---|---|
| Bond Lengths (Å) | | | |
| P-$O_2$ | 1.839 | 1.848 | 1.818 |
| P-$O_3$ | 1.706 | 1.696 | 1.708 |
| P-$O_{4,5}$ | 1.586 | 1.590 | 1.589 |
| P-$O_6$ | 1.783 | 1.782 | 1.808 |
| C-O[b] | 1.43 | 1.43 | 1.43 |
| C-H[b] | 1.09 | 1.09 | 1.09 |
| H-$O_6$[b] | 1.00 | 1.00 | 1.00 |
| Bond Angles (deg) | | | |
| $O_2$-P-$O_3$ ($\theta$) | 90.0 | 90.0 | 90.0 |
| $O_2$-P-$O_{4,5}$ | 90.0 | 90.0 | 90.0 |
| $O_4$-P-$O_5$ ($\phi$) | 135.64 | 135.58 | 133.84 |
| P-O-C[b] ($\psi_2$,$\psi_3$) | 120.0 | 120.0 | 120.0 |
| P-O-H[b] ($\psi_6$) | 120.0 | 120.0 | 120.0 |
| O-C-H[b] ($\alpha$) | 109.5 | 109.5 | 109.5 |
| H-C-H[b] ($\beta$) | 109.5 | 109.5 | 109.5 |
| Dihedral Angles (deg) | | | |
| $C_7$-$O_2$-P-$O_3$ ($\omega_1$) | 60.0 | 180.0 | 60.0 |
| $C_8$-$O_3$-P-$O_2$ ($\omega_2$) | 73.15 | 62.34 | 180.0 |
| H-$O_6$-P-$O_3$ ($\omega_3$) | 300.0 | 300.0 | 180.0 |
| P-$O_{2,3}$-C-H | 180.0 | 180.0 | 180.0 |

[a] See Figure 2 for numbering of atoms. [b] Assumed.

(assuming an axial P-$OCH_3$ bond length of 2.5 Å) were also optimized as also listed in Table V. Later calculations of points along the reaction coordinate showed that a better value for the scissile bond length in the $^-OH$ attack and $MeO^-$ displacement transition states is ~3.0 Å. The general conclusions are not affected by this difference since the relative energies for structures at 2.5 Å parallel those at 3.0 Å (the g,g,−g energies are an exception).

Structures along the reaction path connecting the stable DMP + $^-OH$, the monomethyl phosphate + methoxide, the

**Table IV.** Geometries and Energies for the Dimethoxyphosphorane Transition States during Hydroxide Attack

| parameter[a] | **3a** (g,g, −g) | **3b** (t,g, −g) | **3c** (g,t,t) |
|---|---|---|---|
| | Bond Lengths (Å) | | |
| $P-O_2$ | 1.717 | 1.735 | 1.717 |
| $P-O_3$ | 1.680 | 1.686 | 1.680 |
| $P-O_{4,5}$ | 1.560 | 1.598 | 1.560 |
| $P-O_6$ | 2.50 | 2.50 | 2.50 |
| | Bond Angles (deg) | | |
| $O_2-P-O_3$ ($\theta$) | 94.90 | 95.00 | 94.90 |
| $O_2-P-O_{4,5}$ | 94.50 | 97.50 | 94.50 |
| $O_3-P-O_{4,5}$ | 111.80 | 111.21 | 111.80 |
| $O_3-P-O_6$ | 85.10 | 85.00 | 85.10 |
| $O_4-P-O_5$ ($\phi$) | 134.40 | 133.26 | 134.40 |
| rel energy, kcal/mol | 1.67 | 3.97 | 0.0[b] |

[a] Any parameters not mentioned have same value as in Table III. [b] Total energy for **3c**, −784.407 30 hartrees.

**Table V.** Geometries for the Dimethoxyphosphorane Transition States during Methoxide Displacement

| parameter[a] | **4** (unoptimized)[b] | **4a** (g,g, −g) | **4b** (t,g, −g) | **4c** (g,t,t) |
|---|---|---|---|---|
| | Bond Lengths (Å) | | | |
| $P-O_2$ | 2.50 | 2.50 | 2.50 | 2.50 |
| $P-O_3$ | 1.680 | 1.668 | 1.668 | 1.676 |
| $P-O_{4,5}$ | 1.560 | 1.569 | 1.569 | 1.569 |
| $P-O_6$ | 1.717 | 1.710 | 1.710 | 1.710 |
| | Bond Angles (deg) | | | |
| $O_2-P-O_3$ ($\theta$) | 85.10 | 83.10 | 83.10 | 84.50 |
| $O_2-P-O_{4,5}$ | 85.50 | 83.97 | 83.97 | 83.97 |
| $O_3-P-O_{4,5}$ | 111.80 | 110.68 | 110.68 | 110.68 |
| $O_3-P-O_6$ | 94.90 | 96.90 | 96.90 | 95.50 |
| $O_4-P-O_5$ | 134.40 | 134.95 | 134.95 | 135.37 |

[a] Any parameters not mentioned have same value as in Table III. [b] Unoptimized geometries for displacement transition states derived from the extensively optimized geometry of the g,t,t hydroxide attack transition state, **3c**, with number for atoms 2 and 6 being exchanged.

DMPane, and the transition states were obtained by interpolation (see Table VI). $C_s$ symmetry for the array of five oxygens and phosphorus was assumed throughout the reaction profile. (Thus collinear $^-OH$ attack and $MeO^-$ leaving were assumed.)

All calculations were carried out on a IBM 370/158 computer. The program was compiled using the FORTRAN H compiler at an optimization level of 2. The program was not overlayed after it was determined that less CPU time was required during a given run if a full 800K of core was allocated for the computation.

## Results and Discussion

**Reaction Profile.** Shown in Figure 3 is the reaction profile for the base-catalyzed hydrolysis of dimethyl phosphate in two different ester conformations:

$$(CH_3O)_2PO_2^- + {}^-OH \rightarrow [(CH_3O)_2PO_3H]^{2-} \rightarrow (CH_3O)PO_3H^- + CH_3O^- \quad (1)$$

For a gauche,gauche (g,g) dimethyl phosphate, **1a**, attack of $^-OH$ opposite one of the methoxyl ester bonds can produce only one possible mode of attack, yielding a g,g, −g transition state, **3a**, and DMPane intermediate, **2a**. In contrast attack of $^-OH$ opposite one of the methoxyl ester bonds in the gauche, trans (g,t) DMP structure, **1b**, can proceed via two different reaction paths. Thus $^-OH$ attack opposite the gauche methoxyl ester bond produces a g,t,t transition state, **3c**, and g,t,t DMPane intermediate, **2c**. Attack of $^-OH$ opposite the trans

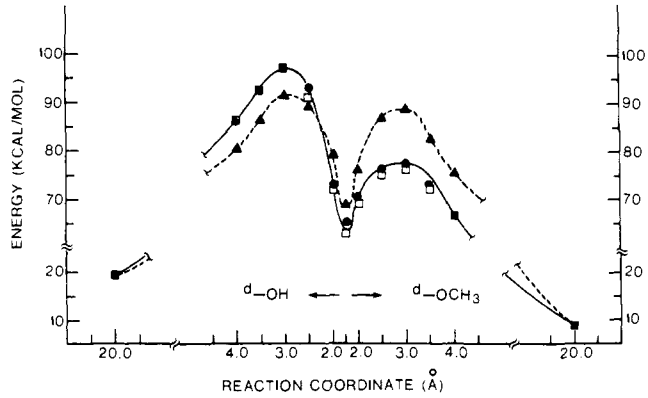


**Figure 3.** Reaction profiles for hydroxide-catalyzed hydrolysis of dimethyl phosphate. The reaction coordinate is defined by the P-OH distance ($d_{OH}$) and P-O(2)$CH_3$ distance ($d_{POCH_3}$) for the attack and displacement steps, respectively. Solid line represents profile for $^-OH$ attack on g,g DMP to yield g,g, −g DMPanes (□) and for $^-OH$ attack on g,t DMP to yield t,g, −g DMPanes (●). Dashed line represents profile for OH attack on g,t DMP to yield g,t,t DMPanes (▲). Geometries are shown in Tables II–VI except that geometries for **4a–c** are the same as **3a–c**, respectively, but with the numbering of atoms 2 and 6 being exchanged.

**Table VI**[a]

| parameter | | | | | |
|---|---|---|---|---|---|
| A. Parameters for Geometry Relaxation during Hydroxide Attack on Dimethyl Phosphate | | | | | |
| 1. (g,t,t) and (g,g, −g) Conformations | | | | | |
| $P-O_6$ | 2.00 | 2.50 | 3.00 | 3.50 | 4.00 |
| $P-O_2$ | 1.790 | 1.717 | 1.666 | 1.666 | 1.666 |
| $P-O_3$ | 1.700 | 1.680 | 1.666 | 1.666 | 1.666 |
| $P-O_{4,5}$ | 1.580 | 1.560 | 1.547 | 1.547 | 1.547 |
| $O_2-P-O_3$ | 91.0 | 94.9 | 94.9 | 94.9 | 94.9 |
| $O_2-P-O_{4,5}$ | 91.4 | 94.5 | 97.4 | 100.3 | 103.0 |
| $O_3-P-O_{4,5}$ | 112.6 | 111.8 | 111.0 | 110.2 | 109.4 |
| 2. (t,g, −g) Conformation | | | | | |
| $P-O_6$ | 2.00 | 3.00 | 3.50 | 4.00 | |
| $P-O_2$ | 1.795 | 1.667 | 1.667 | 1.666 | |
| $P-O_3$ | 1.686 | 1.667 | 1.667 | 1.666 | |
| $P-O_{4,5}$ | 1.598 | 1.567 | 1.557 | 1.540 | |
| $O_2-P-O_3$ | 90.0 | 95.0 | 95.0 | 95.0 | |
| $O_2-P-O_{4,5}$ | 91.9 | 99.9 | 101.7 | 108.4 | |
| $O_{4,5}-P-O_3$ | 111.8 | 110.5 | 110.0 | 108.4 | |
| B. Parameters for Geometry Relaxation during Methoxide Displacement from Dimethoxyphosphorane | | | | | |
| 1. (g,t,t) and (g,g, −g) Conformations | | | | | |
| $P-O_2$ | 2.00 | 2.50 | 3.00 | 3.50 | 4.00 |
| $P-O_6$ | 1.790 | 1.717 | 1.666 | 1.666 | 1.666 |
| $P-O_3$ | 1.700 | 1.680 | 1.666 | 1.666 | 1.666 |
| $P-O_{4,5}$ | 1.580 | 1.560 | 1.547 | 1.547 | 1.547 |
| $O_2-P-O_3$ | 91.0 | 94.9 | 94.9 | 94.9 | 94.9 |
| $O_2-P-O_{4,5}$ | 91.4 | 94.5 | 97.4 | 100.3 | 103.0 |
| $O_3-P-O_{4,5}$ | 112.6 | 111.8 | 111.0 | 110.2 | 109.4 |
| 2. (t,g, −g) Conformation | | | | | |
| $P-O_2$ | 2.00 | 3.00 | 3.50 | 4.00 | 20.00 |
| $P-O_3$ | 1.690 | 1.666 | 1.666 | 1.666 | 1.666 |
| $P-O_{4,5}$ | 1.580 | 1.547 | 1.547 | 1.547 | 1.547 |
| $P-O_6$ | 1.790 | 1.670 | 1.670 | 1.670 | 1.620 |
| $O_2-P-O_3$ | 89.0 | 85.1 | 85.1 | 85.1 | 85.1 |
| $O_2-P-O_{4,5}$ | 88.6 | 82.6 | 79.7 | 77.0 | 72.0 |
| $O_3-P-O_{4,5}$ | 112.6 | 111.0 | 110.2 | 109.4 | 108.0 |

[a] Bond lengths in ångstroms; bond angles in degrees.

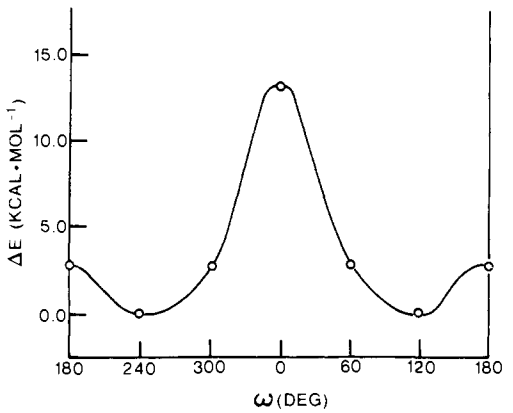


**Figure 4.** Energy vs. P-OH torsional angle, $\omega_3$, for the methoxyl displacement transition state **4** with conformation g,t,$\omega_3$.

bond produces a t,g,−g transition state, **3b,** and t,g,−g DMPane intermediate, **2b.** Note that the conformation about DMPane intermediate, **2b.** Note that the conformation about the hydroxyl bond has been optimized for one of the staggered conformations for each of the three different DMPane intermediates and no geometric relaxation about any of the dihedral angles was permitted during the reaction.

As shown in Figure 3, for all conformations, the reactions are computed to proceed via a metastable pentacovalent intermediate with separate transition states for the (hydroxide) addition and (methoxide) elimination steps. Most significantly, the energy of the transition states is very dependent upon the conformation about the basal methoxyl bond. For the methoxide elimination step, the transition states which have a basal gauche methoxyl group (the t,g, −g or g,g, −g structures) are ca. 11 kcal/mol lower in energy than the transition state with a trans basal methoxyl group (the g,t,t structure).[19] This result agrees nicely with the earlier CNDO and ab initio calculations of bond-order differences in the DMPanes[9,10] and also with the stereoelectronic effect theory. As shown in Figure 2 for the t,g, −g or g,g, −g structures, the basal gauche methoxyl group has one lone pair which is antiperiplanar (app) to the breaking methoxyl bond. In contrast, in the g,t,t structure, **2c** and **4c,** no lone pair is app to the breaking methoxyl bond.

This additional weakening of the apical methoxyl bond by an app lone pair on the basal methoxyl oxygen is likely attributable to mixing of the nonbonding app lone pair with the

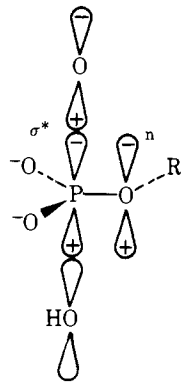


antibonding $\sigma^*$ apical orbital. The effect may alternatively be viewed within a classical resonance description, rather than the above perturbational scheme. In this classical, "anomeric"-type[11,20] picture the no-bond-double-bond resonance structure, **5b,** presumably significantly contributes to the transition-state structures. These considerations suggest that an axial P-O ester bond which is app to a lone pair should be weakened and should have a reduced overlap population.[21] The basal ester bond with the oxygen atom bearing the app lone

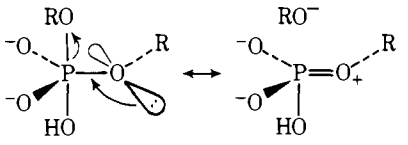


**5**

pair is strengthened and has an enhanced overlap population.

Similarly, stereoelectronic control of the $^-$OH attack transition state is apparent from Figure 3. To describe the app interactions in the $^-$OH attack step we must relabel the torsional angles of the basal ester relative to the *translating* apical bond. Thus in the g,t,t (**3c**) structure, the basal ester bond is cis *to the P-OH bond.* In the t,g, −g (**3b**) and g,g, −g (**3a**) structures the dihedral angle between the basal methoxyl bond and the apical OH bond is 120° or anticlinal (ac). Significantly, for the $^-$OH attack step **3c** is at least 4.0 kcal/mol lower in energy than **3a** or **3b** transition states.[22] The lower energy for the cis transition state relative to the ac transition state is consistent with our earlier finding[9] that two partially app lone pairs (from a cis basal bond) are nearly as effective as a single app lone pair (from a gauche basal bond) in facilitating bond translation. These conclusions for the attack step actually follow directly from a consideration of the principle of microscopic reversibility. Since $^-$OH is chemically similar to $^-OCH_3$, stereoelectronic effects altering the activation energy for $^-$OH translation (attack *or* displacement) must be nearly identical with stereoelectronic effects in $^-OCH_3$ translation (displacement *or* attack).

**Importance of Axial Bond Conformation.** Contrary to our earlier conclusions,[8] the orientation of both the nontranslating *and* translating axial bond is generally not very important in determining the relative transition state energies for the hydrolysis of DMP. Thus, as shown in Figure 4, the methoxyl displacement transition state with gauche methoxyl apical bond and trans methoxyl basal bond has the same energy whether the nontranslating hydroxyl bond is ± gauche or trans. The hydroxyl ± ac conformation is 2.8 kcal/mol lower in energy than the staggered conformation but this is likely attributable to intramolecular hydrogen bonding to the basal $O^-$ (overlap population and charge-density comparisons confirm this conclusion). The very high energy for the cis hydroxyl conformation is attributable to severe steric interaction between the coplanar basal O-$CH_3$ and O-H groups ($d_{CH_3\text{-}HO}$ = 1.83 Å).

In addition, as shown in the reaction profiles of Figure 3 and Table VIII, little difference in transition-state energies is found for conformations differing only in rotation about the translating apical bond. (This is true for *both* steps of the reaction.) Previously, based upon overlap population comparisons, it was felt that a trans axial bond should be weaker than a gauche axial bond.[9] A lone pair on the gauche axial bond is app to the basal methoxyl bond and should lead to an increase in the overlap population in the axial bond. Again, this is a manifestation of the "anomeric type" double-bond-no-bond resonance picture for the stereoelectronic effect: the bond opposite to the app lone pair has some "no-bond" resonance character

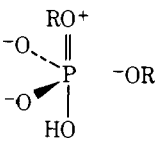


**6**

to it; the bond containing an app lone pair has some "double-bond" character to it. The double-bond contribution should increase the axial bond overlap population and presumably

**Table VII.** Ab Initio Energies and Population Analysis for the Dimethoxyphosphorane Intermediates

| | conformation | | |
|---|---|---|---|
| | **2a** (g,g, −g) | **2b** (t,g, −g) | **2c** (g,t,t) |
| rel energy,[a] kcal/mol | 0.0 | 2.53 | 6.24 |
| bond | overlap population | | |
| $P-O_2$ | 0.2141 | 0.2102 | 0.2276 |
| $P-O_3$ | 0.3067 | 0.3188 | 0.3190 |
| $P-O_4$ | 0.4548 | 0.4529 | 0.4513 |
| $P-O_5$ | 0.4602 | 0.4547 | 0.4550 |
| $P-O_6$ | 0.2537 | 0.2533 | 0.2386 |

[a] Total energy of (g,g, −g) conformation, −784.449 94 hartrees.

strengthen this bond. We describe this as a "counterbalancing" stereoelectronic effect.

In order to further appreciate these interactions, we make more explicit use of one-electron MO theory.[23] The interaction of a doubly occupied MO (such as the app lone pair orbital, $\phi_n$) with a vacant MO (such as the antibonding orbital, $\phi_{\sigma^*}$) yields a two-electron stabilization energy:

$$SE \approx 2K^2 S_{n\sigma^*}{}^2/\Delta E_{n\sigma^*} \qquad (2)$$

Here, $S_{n\sigma^*}$ is the overlap integral of $\phi_n$ and $\phi_{\sigma^*}$ and $\Delta E_{n\sigma^*}$ is the energy separating these orbitals. From eq 2 this stabilization energy increases with increasing overlap, $S_{n\sigma^*}$, and decreasing energy separation, $\Delta E_{n\sigma^*}$, between the interacting orbitals. The app lone pair stereoelectronic effect presumably derives from this equation since maximal overlap between n and $\sigma^*$ is found for the app orientation.[5,7,11,23,24] The reason that the transition-state energies are insensitive to the translating axial bond conformation likely reflects the difference in bond lengths between the basal and the scissile axial bonds. The basal methoxyl bond length is 1.67 Å while the scissile apical methoxyl bond length is 2.50 Å. The orbital interaction picture for the "counterbalancing" stereoelectronic effect requires effective overlap of the nonbonding lone-pair orbital on the axial methoxyl oxygen with the basal methoxyl $\sigma^*$ orbital (structure **6**). Increasing the separation between phosphorus and the oxygen atom bearing the lone pair will diminish this overlap, $S_{n\sigma^*}$, reduce the stabilization energy of eq 2, and reduce the counterbalancing stereoelectronic effect. On the other hand, increasing the distance between phosphorus and the axial oxygen should lower the energy of the axial $\sigma^*$ orbital, hence *decrease* the energy separation, $\Delta E_{n\sigma^*}$, and increase the SE produced by the normal stereoelectronic effect[25] (depicted in structure **5**). These conclusions are confirmed below in comparisons of overlap population changes.

**Overlap Populations.** Apart from our earlier communication[10] all previous theoretical attempts to assess the importance of the app lone pair stereoelectronic effect have utilized overlap population and bond-length comparisons.[5-7] It is significant that, while the major qualitative conclusions based upon these comparisons are supported by our actual transition state energy calculations, important differences exist and highlight the uncertainty that should be placed upon conclusions deduced only from overlap population comparisons. The overlap population of a bond which is app to a lone pair is always smaller than the overlap population of a bond which is not app to a lone pair (assuming that we are comparing otherwise identical structures). In the DMPs (Table VII, ref 8) the overlap population of a bond app to a lone pair is 0.3309 (for a g,t conformation) or 0.3348 (for a g,g conformation), while the overlap population of a bond not app to a lone pair is 0.3419 (for a t,t conformation) or 0.3479 (for a g,t conformation). As discussed above and previously[8] the differences in the g,g and g,t structures include the counterbalancing bond-strengthening, "double-bond" interaction as well and partially obscure direct comparisons. In the DMPane intermediates, Table VII, the axial methoxyl bond overlap populations are 0.2276 (for g,t, −t with no app lone pairs), 0.2141 (for g,g, −g with one app lone pair), and 0.2102 (for t,g, −g with one lone pair). For the methoxyl elimination transition states, Table VIII, the axial methoxyl overlap populations are 0.0414 (for g,t, −g with no app lone pairs), 0.0365 (for t,g, −g with one app lone pair), and 0.0387 (for g,g, −g with one app lone pair). Although the absolute difference in the overlap populations between conformations is smaller in the transition states, the *percentage* change in the overlap population of a bond with or without an app lone pair is *greater* in the transition states than in the ground state or metastable intermediates. Thus the overlap population of a bond with an app lone pair is 95-96% smaller than a bond without an app lone pair for the DMPs, 92-94% smaller for the DMPanes, and 88-93% smaller for the transition states. The increasing significance of the stereoelectronic effect in going from ground state to intermediate to transition state is consistent with the increased mixing of n and $\sigma^*$ orbitals as the $\sigma^*$ orbital energy is decreased with an increase in the $P-OCH_3$ bond length (1.43 Å in DMP, 1.67 Å in DMPane, and 2.5 Å in the transition state).

The energy differences between the conformations are also sensitive to the magnitude of the stereoelectronic effect (as represented by the percentage changes in the overlap populations). Thus in DMP with only small overlap population changes (~ca. 5%) the energy difference between the conformations is less than 1 kcal/mol. In DMPane with overlap population changes of 6-8% the energy difference between the conformations is 2-6 kcal/mol. In the transition states with 7-12% overlap population changes, the energy differences are

**Table VIII.** Ab Initio Energies and Population Analysis for the Dimethoxyphosphorane Transition States of the Methoxide Displacement Step

| | conformation[a] | | | | |
|---|---|---|---|---|---|
| | **4a** (g,g, −g) | **4b** (t,g, −g) | **4c** (g,t,t) | **4d** (g,t, −g) | **4e** (g,t, −t) |
| rel energy[a] kcal/mol | 0.0[b] (0.0)[c,d] | 0.73 (0.67)[d] | 11.33 (11.26)[d] | 11.55 | 8.73 |
| bond | | | | | |
| $P-O_2$ | 0.0387 | 0.0365 | 0.0409 | 0.0414 | 0.0408 |
| $P-O_3$ | 0.3388 | 0.3460 | 0.3481 | 0.3335 | 0.3432 |
| $P-O_4$ | 0.4646 | 0.4649 | 0.4615 | 0.4629 | 0.4615 |
| $P-O_5$ | 0.4687 | 0.4671 | 0.4621 | 0.4709 | 0.4677 |
| $P-O_6$ | 0.3159 | 0.3140 | 0.3079 | 0.3073 | 0.3120 |

[a] Only **4b** and **4c** were geometry optimized. **4a, 4d,** and **4e** used geometry optimized for **4b.** [b] Total energy of **4a**, −784.430 73 hartrees. [c] Total energy of **4a** with standard geometry used for Figure 3, −784.429 36 hartrees. [d] Relative energy using standard unoptimized geometry for **4** in Table V.

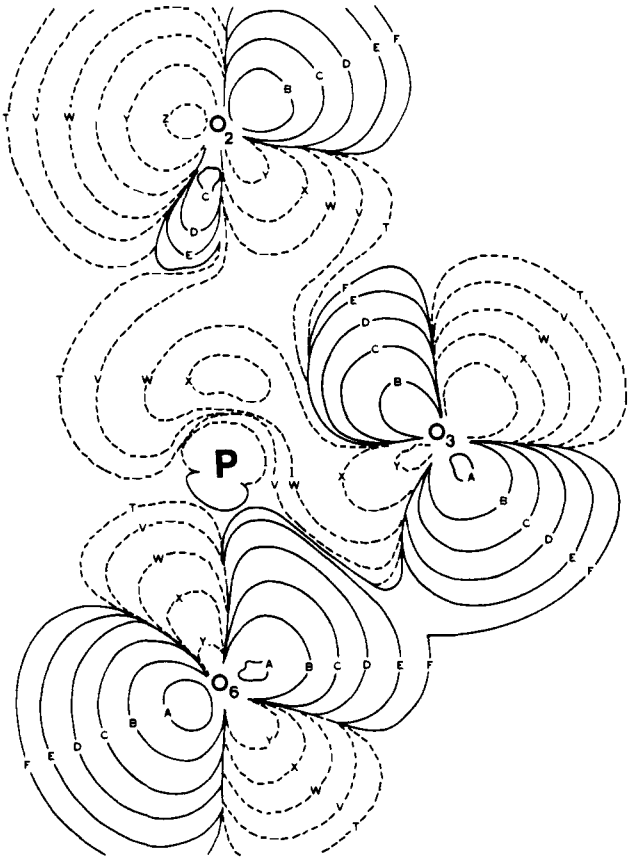


**Figure 5.** Electron density difference map of the top 11 highest occupied molecular orbitals in the **4b** vs. **4c** transition states. Solid lines represent higher electron density in **4b**, while dashed lines represent higher electron density in **4c**. The A through F contour lines represent 0.5, 0.125, 0.0313, 0.007 81, 0.001 95, and 0.000 488 electron density, respectively, and the T through Z contour lines represent −0.000 488, −0.001 95, −0.007 81, −0.0313, −0.125, and −0.5 electron density, respectively.

8–11 kcal/mol. Of course, if the stereoelectronic effect did not have its major impact in the transition state, little activation-energy differences and no kinetic acceleration would result from these interactions.

Beyond these gross first-order effects, more detailed correlations of overlap-population differences and relative energies for the conformations appear not to be valid. Thus, from stereoelectronic considerations the trans bond in t,g DMP and the trans axial methoxyl bond in the t,g, −g DMPane should be the weakest bonds. Yet in the methoxyl displacement transition state it is the g,g, −g structure (**4a**) which has the lowest energy. Thus, the t,g, −g transition state with trans axial methoxyl group is 0.7 kcal/mol higher in energy in spite of the fact that it has a slightly lower overlap population than the g,g, −g transition state. This energy order also does not fit the counterbalancing, bond-strengthening stereoelectronic effect. Apparently with geometry optimization, other effects also significantly perturb the overlap populations besides the stereoelectronic effect. (However, the energy difference between the conformations is not affected significantly by geometry optimization, Table VIII). Caution must thus be raised in interpretation of smaller overlap-population and energy differences. Lehn and Wipff[5,6] have argued that an important component of the app lone pair stereoelectronic effect was the strengthening of the bond containing the app lone pair (due to what we have described as the "counterbalancing" stereoelectronic effect). We want to emphasize that this is likely only a *ground-state effect*. In transition states with much longer leaving-group bonds (such as the axial bond in a trigonal bipyramidal structure) this "counterbalancing effect" is negligible and hence *cannot* alter reactivity.

As pointed out by Dr. G. Wipff (personal communication) the counterbalancing stereoelectronic effect could still be important for tetrahedral carbon species. In contrast to the tetrahedral structures, in the trigonal bipyramid geometry the axial oxygens' lone pairs in any of the staggered conformations can always interact with the three basal oxygen–phosphorus bonds. However, as discussed earlier,[8] the counterbalancing stereoelectronic effect between an axial oxygen lone pair and the anionic phosphoryl bonds should not be as important as between an axial oxygen lone pair and the basal (neutral) P-$OCH_3$ bond. Finally, if the phosphorane transition state in solution is much earlier than predicted by the gas-phase calculations, then the counterbalancing effect could still play a role in the reactions of phosphates as well.

The effect of the app lone pairs on the scissile P-$OCH_3$ bond overlap populations is seen readily in the electron density difference map in Figure 5. Here the electron density in the top 11 highest occupied molecular orbitals (largely strongly mixed oxygen lone pairs) of the g,t,t transition state, **4c**, for the methoxide leaving step has been subtracted from the t,g, −g transition state, **4b**. The two-dimensional projection represents the plane containing $O_2$,P,$O_3$,$O_6$. The P-$O_2$ bond-weakening effect of the app lone pair on $O_3$ in the t,g, −g conformer is shown clearly by the dashed contour lines representing lower electron density in t,g,−g vs. g,t,t. The stereoelectronic, bond-strengthening interaction between phosphorus and $O_3$ is shown by the solid line representing increased $\pi$-type electron density in the t,g, −g transition state. The difference map thus supports the qualitative double-bond–no-bond resonance picture **5b**.

**Steric Effects.** An argument could be raised that the app lone pair stereoelectronic effect could really be interpreted in terms of a simple steric effect. Thus, it is not unreasonable that the methoxyl displacement transition state with a trans basal bond is higher in energy than a transition state with a gauche basal bond because the trans structure will have an unfavorable steric interaction between the cis/eclipsed basal O-$CH_3$ bond and the axial P-OH bond. However, the eclipsing steric interaction should be at least as important in the metastable DMPanes where the bond lengths are shorter. Here steric interactions are no greater than 4 kcal/mol (comparing **2b** and **2c**, Table III) and could be even less if stereoelectronic effects are partially responsible for these energy differences. The 8–11 kcal/mol differences in the transition-state energies must therefore arise from some factor other than steric effects.

## Conclusions

These calculations provide further support for the app lone pair stereoelectronic effect theory. Deslongchamps[2] has shown that the breakdown of tetrahedral carbon species operates under stereoelectronic control and Pople and Lehn have demonstrated in related calculations similar effects.[5–7]

The DMPane reaction profile calculations have shown the energy of a trigonal bipyramidal pentacovalent transition state is critically dependent upon the orientation of the basal ester bond. In fact, for the stereoelectronic effect to alter the rate of a two-step reaction in which both attack and displacement steps are partially rate limiting, *rotation about the basal ester bond during the reaction is essential.* Otherwise, while an app lone pair on a basal ester bond will facilitate attack, without rotation a lone pair will not be app to the leaving group. Hence the overall activation energy for the reaction will be essentially unaltered. Only with rotation about the equatorial ester bond during the reaction can the stereoelectronic effect lower the activation barrier for *both* steps and hence lower the overall activation barrier.

This rotation *during* reaction is not feasible for a concerted

$S_N2$-type displacement reaction where the rotation rate will only be a fraction of the rate of translation across the top of the energy barrier.[26] While an app lone pair effect could facilitate the first, largely attack phase of the reaction, the latter, largely displacement stage of a single barrier pathway cannot be helped by the now cis lone pair. We expect therefore that the app lone pair effect cannot play an important role in $S_N2$-type reactions. If, however, an intermediate, no matter how high its energy, exists along the reaction pathway, bond rotation is allowed and "stereoelectronic catalysis" of both bond making and breaking is possible. The intermediate need only have a lifetime of a single bond rotation. Displacement reactions at tetrahedral carbon ($S_N2$ type) cannot be stereoelectronically catalyzed while those at tetrahedral phosphorus (and other second- and third-row elements) may well obey these principles since pentacovalent intermediates are realizable. In fact, we have suggested that these effects are responsible for much of the 6 kcal/mol extra stabilization of the five-membered cyclic vs. acyclic phosphate diester transition states.[9] The substantial 5–11 kcal/mol lowering of the transition-state energies for favorable app lone pair interactions shown in Figure 3 demonstrates that effects large enough to account for the experimental observations may well be possible.

While app effects should not be important for carbon $S_N2$ reactions, they should operate in reactions involving trigonal or tetrahedral centers such as $S_N1$ and acyl/addition/elimination reactions. The trigonal or tetrahedral intermediates in these reactions will generally have lifetimes long enough to permit single-bond rotation. Our interpretation of the lysozyme catalyzed hydrolysis of an acetal[8] and Deslongchamp's experimental verification of the stereoelectronic effect in the hydrolysis of amides and other systems[2] do not violate this requirement for bond rotation.[2]

**Acknowledgment.** Support of this research by NSF, NIH, the Alfred P. Sloan Foundation, and the International Fulbright Commission is gratefully acknowledged. We also thank the Computer Center, University of Illinois at Chicago Circle, for generous allocation of computing time.

## References and Notes

(1) Fellow of the Alfred P. Sloan Foundation, 1975–1979; Fulbright Senior Fellow, 1978.
(2) P. Deslongchamps and R. J. Taillerfer, *Can. J. Chem.*, **53**, 3029 (1975), and references cited therein.
(3) D. R. Storm and D. E. Koshland, Jr., *J. Am. Chem. Soc.*, **94**, 5815 (1972).
(4) W. L. Mock, *Bioorg. Chem.*, **4**, 270 (1975).
(5) J. M. Lehn and G. Wipff, *J. Chem. Soc., Chem. Commun.*, 800 (1975).
(6) (a) J. M. Lehn and G. Wipff, *J. Am. Chem. Soc.*, **96**, 4048 (1974); (b) *ibid.*, **98**, 7498 (1976); (c) *Helv. Chim. Acta*, **61**, 1274 (1978).
(7) (a) L. Radom, W. J. Hehre, and J. A. Pople, *J. Am. Chem. Soc.*, **94**, 2371 (1972). (b) G. A. Jeffrey, J. A. Pople, and L. Radom, *Carbohydr. Res.*, **25**, 117 (1972), have provided further support for these anomeric-type effects by noting that the calculated bond lengths agree with the expected overlap population changes.
(8) D. G. Gorenstein, J. B. Findlay, B A. Luxon, and D. Kar, *J. Am. Chem. Soc.*, **99**, 3473 (1977).
(9) D. G. Gorenstein, B. A. Luxon, J. B. Findlay, and R. Momii, *J. Am. Chem. Soc.*, **99**, 4170 (1977).
(10) D. G. Gorenstein, B. A. Luxon, and J. B. Findlay, *J. Am. Chem. Soc.*, **99**, 8049 (1977).
(11) S. David, O. Eisenstein, W. J. Hehre, L. Salem, and R. Hoffman, *J. Am. Chem. Soc.*, **95**, 3806 (1973), and references cited therein.
(12) R. L. Collin, *J. Am. Chem. Soc.*, **88**, 3281 (1966).
(13) D. B. Boyd, *J. Am. Chem. Soc.*, **91**, 1200 (1969).
(14) A. Rauk, L. C. Allen, and K. Mislow, *J. Am. Chem. Soc.*, **94**, 3035 (1972).
(15) C. A. Deakyne and L. C. Allen, *J. Am. Chem. Soc.*, **98**, 4076 (1976).
(16) R. Hoffmann, J. M. Howell, and E. L. Muetterties, *J. Am. Chem. Soc.*, **94**, 3047 (1972).
(17) (a) W. J. Hehre, W. A. Lathan, R. Ditchfield, M. D. Newton, and H. A. Pople, Quantum Chemistry Exchange Program, No. 236; (b) D. L. Lichtenberger and R. F. Fenske, QCPE Program No. 310.
(18) W. J. Hehre, R. F. Stewart, and J. A. Pople, *J. Chem. Phys.*, **51**, 2659 (1969).
(19) As shown in Table VIII, this result is independent of the level of geometry optimization.
(20) (a) E. A. C. Lucken, *J. Chem. Soc.*, 2954 (1959); (b) C. Romers, C. Altona, H. R. Buys, and E. Havinga, *Top. Stereochem.*, **4**, 39 (1969).
(21) R. S. Mulliken, *J. Chem. Phys.*, **36**, 3428 (1962).
(22) Only the structure for the higher energy transition state (t,g, −g) in the $^-$OH attack step was fully geometry optimized. The other transition-state conformers for $^-$OH attack used interpolated geometric parameters and thus the energy separation between the transition-state conformational isomers should only *increase* if full geometry optimization was performed on the lower energy structures as well.
(23) W. T. Borden, "Modern Molecular Orbital Theory for Organic Chemists", Prentice-Hall, Englewood Cliffs, N.J., 1975.
(24) (a) N. D. Epiotis, W. R. Cherry, S. Shaik, R. L. Yates, and F. Bernardi, *Top. Curr. Chem.*, **70** (1977); (b) L. Radom, J. A. Pople, V. Buss, and P. v. R. Schleyer, *J. Am. Chem. Soc.*, **92**, 6380 (1970); (c) F. R. Jensen and B. E. Smart, *ibid.*, **91**, 5686 (1969); (d) I. J. Broxton, L. W. Deady, A. R. Katritzky, A. Lin, and R. D. Topsin, *ibid.*, **92**, 6845 (1970).
(25) On the other hand, charge-transfer effects in the transition state should partially oppose these changes. Thus with increasing charge transfer as the P–$O_2$ bond lenghtens the app 1p orbital on $O_3$ should lower in energy while the P–$O_2$ $\sigma^*$ orbital should raise. This will increase $E_{n\sigma^*}$ and decrease the SE. Similarly charge transfer should increase the counterbalancing stereoelectronic effect.
(26) W. J. Chesnavich and M. T. Bowers, *J. Am. Chem. Soc.*, **98**, 8301 (1976).
(27) The numerous conformational states widely observed for enzyme–substrate complexes may well reflect the requirement of the enzyme to achieve optimal app lone pair interactions during each of the multistep reactions.